

Article

The Oxidation Properties of a NiCrAlY Coating Fabricated by Arc Ion Plating

Lei Huang¹, Zhaohui Zhou², Lanlan Yang^{2,*} and Yanxin Qiao^{2,*} ¹ Luoyang Ship Material Research Institute, Luoyang 471023, China² School of Materials Science and Engineering, Jiangsu University of Science and Technology, Zhenjiang 212003, China

* Correspondence: lanlanyang@just.edu.cn (L.Y.); yxqiao@just.edu.cn (Y.Q.)

Abstract: The microstructures, phase compositions, and high-temperature oxidation behavior of a NiCrAlY coating fabricated by arc ion plating were investigated by scanning electron microscopy (SEM), energy dispersive spectrometer (EDS), atomic force microscope (AFM), and X-ray diffractometer (XRD). The results indicate that the NiCrAlY coating was covered by a protective Al₂O₃ scale with excellent oxidation resistance after oxidation at 1050 °C for 100 h; the β phase rich in Al in the as-deposited coating was transformed into a γ/γ' phase; the interdiffusion zone (IDZ), secondary reaction zone (SRZ), and needle-like TCP phases were detected in the superalloy substrate beneath the coating.

Keywords: Ni-based single-crystal superalloy; NiCrAlY coating; high-temperature oxidation; Al₂O₃ scale; TCP phases



Citation: Huang, L.; Zhou, Z.; Yang, L.; Qiao, Y. The Oxidation Properties of a NiCrAlY Coating Fabricated by Arc Ion Plating. *Coatings* **2023**, *13*, 22. <https://doi.org/10.3390/coatings13010022>

Academic Editors: Philipp Vladimirovich Kiryukhantsev-Korneev, Giorgos Skordaris and Emerson Coy

Received: 16 November 2022

Revised: 13 December 2022

Accepted: 16 December 2022

Published: 22 December 2022



Copyright: © 2022 by the authors. Licensee MDPI, Basel, Switzerland. This article is an open access article distributed under the terms and conditions of the Creative Commons Attribution (CC BY) license (<https://creativecommons.org/licenses/by/4.0/>).

1. Introduction

Single-crystal superalloys are adopted in hot sections of aeroengine owing to their elevated mechanical properties [1]. Single-crystal superalloys were developed quite recently. René N5, DD6, PWA1484, etc., with large amounts of refractory elements, are widely adopted at present. When it is in service, the corrosion behavior of the superalloy occurs. Elements like Al, Cr, and Ta are lost, which destroys the mechanical properties of the superalloy at high temperature. Considering the operation surroundings of the single-crystal superalloy, only composite materials are able to meet the harsh requirements; the necessary mechanical properties are offered by the single-crystal superalloy, and the protection against oxidation or corrosion is furnished by high-temperature coatings [2,3]. The anti-corrosion elements in the coating, such as Al, will react with the corrosion medium, and an Al₂O₃ scale is formed. The Al₂O₃ scale is not only able to isolate corrosive media from the coating and superalloy, but also is very stable and an excellent protective scale at high temperature. Among all kinds of high-temperature protective coatings, MCrAlY (M = Ni, Co, or Ni and Co) coating can be adopted as a standalone coating and as the bond coating of thermal barrier coatings (TBCs) [4–8]. For the MCrAlY coating, M is the main element, which is used to match with the substrate superalloy; Al is oxidized to Al₂O₃, whose content is about 7–16 wt.%; Cr, with a content of 15–35 wt.%, improves the corrosion resistance of the coating. With the addition of the rare-earth element Y, the purity and adhesion of the Al₂O₃ scale is significantly improved. Consequently, the oxidation and corrosion resistance of the MCrAlY coating are excellent at high temperature. In addition, the chemical compositions of the MCrAlY coating can be flexibly adjusted as required. For instance, Re, Ta, Pt, etc., are added into the coating according to the service conditions [9–11].

An early technology to obtain MCrAlY coatings with high density, strong bonding force, and excellent oxidation resistance was electron beam physical vapor deposition (EB-PVD) [12]. When the EB-PVD technology is adopted to prepare coatings, alloy targets

are mostly used. Therefore, the coating composition is affected by the target composition. It should be noted that a high-energy ion beam bombards the target; this melts, sublimates, evaporates, and finally deposits the target on the substrate. At last, a coating is obtained. It should be noted that the saturated vapor pressure of each element in this process is different, so the composition of the coating deposited on the sample surface will change. Therefore, the coating composition is hard to control with this technology. As thermal spraying technology develops, the coating compositions become more easily adjusted, and the deposition efficiency can be improved [13,14]. However, powders will be oxidized, and oxide inclusions will be formed during the spraying process. To eliminate the oxides in the coating, magnetron sputtering and arc ion plating (AIP) technology have been adopted [15–18]. The columnar grains are obtained by magnetron sputtering. The corrosive medium invades into the coating through the columnar grain boundary; then, the oxidation and corrosion resistance are reduced. Different from the magnetron sputtering, coatings prepared by AIP exhibit equiaxed grains. Therefore, the diffusion path of the corrosive medium is greatly extended, and the service life and the corrosion resistance of the coating are improved.

In this paper, the microstructure and oxidation behavior of NiCrAlY coatings fabricated by AIP are investigated. The phase transition during the oxidation process and the effect of elemental interdiffusion between the coating and the substrate superalloy on the microstructure of the superalloy are explored, with the aim to lay the foundation for the application of coatings fabricated by AIP.

2. Experimental Procedures

Ni-based single-crystal superalloy René N5 was chosen as the substrate superalloy. Its nominal chemical compositions are listed in Table 1. Because the total content of refractory elements (Ta, Mo, W, Re) in this superalloy is about 16 wt.%, its high-temperature mechanical properties are excellent. The Al content is 6.2 wt.%, and the Cr content is 7 wt.%, to ensure its oxidation and corrosion resistance. The superalloy was machined into $\Phi 15 \times 2$ mm by WEDM, ground with 2000# SiC paper, and degreased with an ultrasonic cleaner in a mixture of ethanol and acetone with a volume ratio of 3:1 for 20 min, then dried before coating deposition. Arc ion plating (Model DH15, Beiyu, Shenyang, Liaoning, China) was used to fabricate the NiCrAlY coating, the targeted nominal chemical compositions of which are listed in Table 1. Specific deposition parameters can be seen in reference [17]. An annealing treatment of the NiCrAlY coating was conducted at 1050 °C in a vacuum ($<6 \times 10^{-3}$ Pa) for 4 h.

Table 1. Nominal chemical compositions of René N5 superalloy and NiCrAlY target (wt.%).

	Ni	Co	Cr	Al	Ta	Mo	W	Re	Hf	C	B	Y
N5	Bal.	7.5	7	6.2	6.5	1.5	5	3	0.15	0.05	0.004	0.01
NiCrAlY	Bal.		27	11								0.5

The oxidation test was carried out in a muffle furnace (Luoyang Kere Furnances Co., LTD., Luoyang, Henan, China) set at 1050 °C. The surface areas of the superalloy and the coated ones were calculated by measuring the diameter and height of these samples with a vernier caliper. The samples were placed into the crucibles with a purity of 99.99 wt.% alumina, and the crucibles containing the samples were put in the muffle furnace set at 1050 °C. The samples were removed from the crucibles at eight points of oxidation time: 0 h, 5 h, 10 h, 20 h, 40 h, 60 h, 80 h, 100 h. They were then weighed with an electronic balance with a sensitivity of 0.01 mg after cooling to room temperature. The microstructures, chemical compositions, and phase components of the NiCrAlY coating and the N5 superalloy before and after oxidation were characterized by SEM (scanning electron microscopy, Inspect F 50, FEI Co., Hillsboro, CA, USA), EDS (energy dispersive spectrometer, X-Max, Oxford instruments Co., Oxford, UK), AFM (atomic force microscope, NAVITAR, N9410S, CA,

USA), and XRD (X-ray diffractometer, X'Pert PRO, PANalytical Co. Almelo, Holland, Cu K α radiation at 40 kV).

3. Results and Discussion

AFM and SEM results showing the microstructures of the NiCrAlY coating fabricated by arc ion plating (AIP) are shown Figure 1. The coating presents a rough surface. Cauliflower-like patterns and large droplets can be observed, as shown in Figure 1a,b. The thickness of the NiCrAlY coating is about 29 μm . An interface between the coating and the René N5 superalloy is clearly identified by a red line shown in Figure 1c. It is obvious that the microstructure of the superalloy has not been changed, which means that the deposition process by AIP and the annealing process did not affect the superalloy underneath.

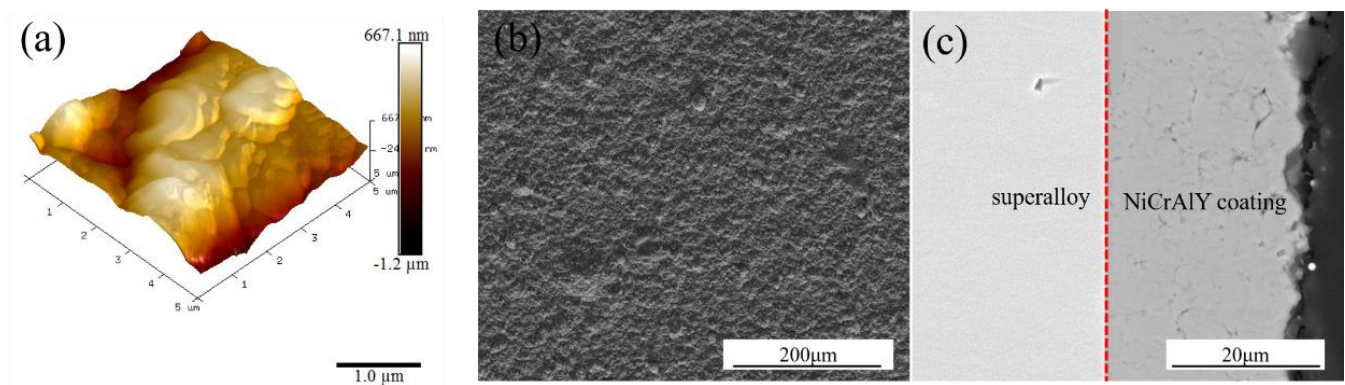


Figure 1. Microstructures of the NiCrAlY coating shown by AFM and SEM: (a) AFM (b) and (c) SEM.

Figure 2 is the XRD pattern of the NiCrAlY coating. The main phases in the coating are γ/γ' , β -NiAl, and α -Cr phases, which can be inferred from the XRD pattern. It should be noted that the Al content in the β -NiAl phase is high, and the Cr content in the α -Cr phase is high. During service at high temperature, the high contents of Al and Cr help to form a protective oxide scale, such as Al_2O_3 or Cr_2O_3 . Therefore, the coating exhibits excellent oxidation and corrosion resistance.

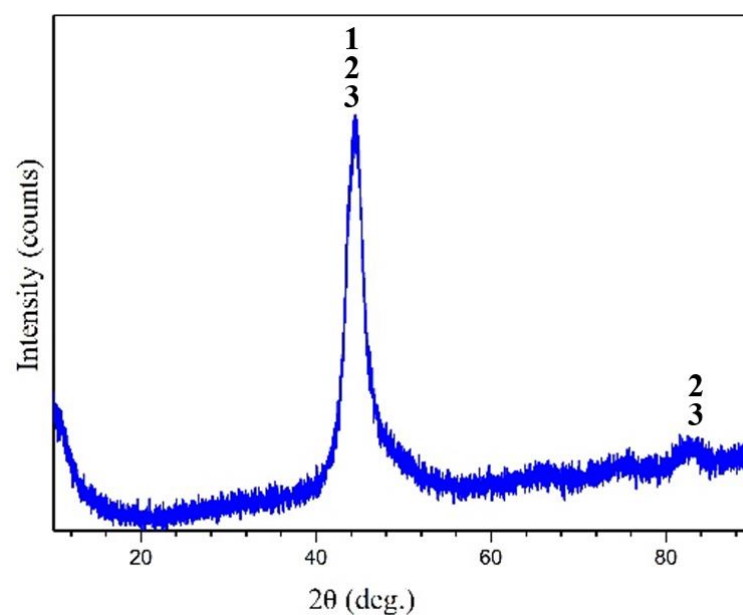


Figure 2. XRD pattern of the NiCrAlY coating fabricated by AIP (1- γ/γ' , 2- β -NiAl, and 3- α -Cr).

The oxidation kinetics of the NiCrAlY coating and the René N5 superalloy at 1050 °C are shown in Figure 3a. As time passes, the oxidation mass gain of the NiCrAlY coating and the superalloy clearly increase at 1050 °C. The mass gain of the NiCrAlY coating is higher than that of the superalloy. After oxidation from 0 h to 20 h, their mass gains increase rapidly. After oxidation for 20 h, the mass gain of the coating and the superalloy reached 0.3746 and 0.1554 mg/cm². Then, they slow down quickly. After oxidation for 100 h, the oxidation mass gain of the coating and the René N5 superalloy reached 0.53186 and 0.31877 mg/cm², respectively. We investigated whether they follow the parabolic law:

$$y^2 = kt \quad (1)$$

where y is the oxidation mass gain, k is the parabolic rate constant, and t is the oxidation time. The function relationship of y^2 vs. t is plotted in Figure 3b. To avoid the effect of initial oxidation, the points at 5 h and 10 h of oxidation are ignored. It can be seen that the NiCrAlY coating and the substrate superalloy follow the parabolic law. The parabolic rate constants of the coating and the superalloy are 1.79×10^{-3} and 6.41×10^{-4} mg² cm⁻⁴ h⁻¹, respectively.

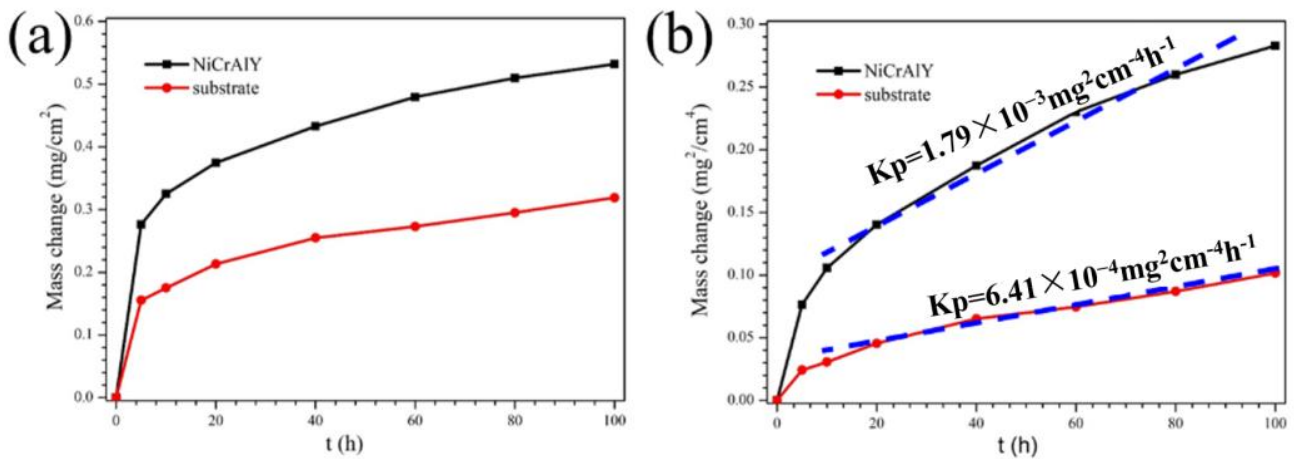


Figure 3. Oxidation kinetics of the NiCrAlY coating and the substrate superalloy after oxidation at 1050 °C: (a) y vs. t and (b) y^2 vs. t .

Figure 4 exhibits the XRD patterns of the NiCrAlY coating and the René N5 superalloy after oxidation at 1050 °C for 100 h. After oxidation for 100 h, the main oxide products on the superalloy are α -Al₂O₃, NiAl₂O₄, and Ta₂O₅. Among these products, the protectiveness of α -Al₂O₃ is excellent. But NiAl₂O₄ and Ta₂O₅ exhibit poor performance. The coefficients of thermal expansion for the three oxides are different, especially between α -Al₂O₃ and Ta₂O₅ [19,20]. This resulted in the formation of pores and cracks. These means that the oxidation resistance of the superalloy is poor, which is consistent with Ren's [21] and Wang's studies [22,23]. For the NiCrAlY coating, only α -Al₂O₃ is detected on the surface after oxidation for 100 h. It should be noted that the γ and γ' phases, not β -NiAl (rich in Al) or α -Cr (rich in Cr), were tested in the coating. This means that the β -NiAl phase in the as-deposited coating has been transferred into γ/γ' phases during oxidation at 1050 °C. The formation of α -Al₂O₃ consumes a large amount of Al in the coating, so the β -NiAl phase in the as-deposited coating is transferred into γ/γ' phases, whose Al content is low. The existence of Cr in the coating can help the formation of α -Al₂O₃ [17,23,24]. Therefore, the presence of the NiCrAlY coating improves the oxidation resistance of the N5 superalloy.

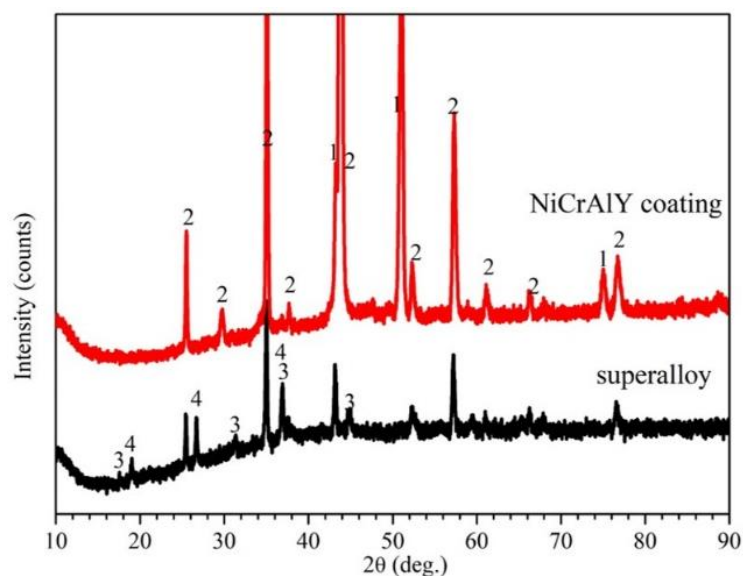


Figure 4. XRD patterns of the NiCrAlY coating and the superalloy after oxidation at 1050 °C for 100 h (1- γ/γ' , 2- α - Al_2O_3 , 3- NiAl_2O_4 , and 4- Ta_2O_5).

The surface and cross-sectional microstructures of the N5 superalloy after oxidation at 1050 °C for 100 h are shown in Figure 5. Although the oxidation weight gain and parabola constant of the superalloy are relatively low, this does not mean that its oxidation resistance is excellent. A spallation spot is detected, which is indicated by red arrows and red dotted ellipses in Figure 5a, b. There is a large number of white particles dispersing on the superalloy surface, indicated by orange arrows in Figure 5a, which is referred to as Ta_2O_5 [22–27]. These Ta_2O_5 particles can be detected on the surface of the oxide scale and in the oxide scale near the interface, as shown in Figure 5b. The oxide scale is divided into two parts: the grey one and the dark one. In fact, there is a competitive relationship between Ta and Al in the superalloy during oxidation at high temperature, which affects the oxidation process of Al. The final result is that the formed Al_2O_3 scale is incomplete, with cracks and spallation spots. Combined with the XRD patterns in Figure 4, the grey part is mainly composed of NiAl_2O_4 , and the dark one is composed of α - Al_2O_3 [26,27]. The internal oxidation is detected beneath the oxide scale, indicated by the black arrow in Figure 5b. The above results indicate that the oxidation resistance of the superalloy must be improved, which is consistent with the research by Ren [21] and Wang [22,23]. What is more, internal oxidation is detected in the superalloy. All of this indicates that the oxidation resistance of the superalloy must be improved by applying the high-temperature protective coating.

Figures 6 and 7 show the surface and cross-sectional morphologies of the NiCrAlY coating after oxidation at 1050 °C for 100 h. It is obvious that the NiCrAlY coating is covered by a dense α - Al_2O_3 scale. No spallation or cracks are detected on the NiCrAlY coating's surface after oxidation at 1050 °C for 100 h, as shown in Figure 6. The Al_2O_3 scale is continuous, complete, and about 1.59 μm in thickness, as shown in Figure 7. It should be noted that some white particles are detected in the Al_2O_3 scale near the coating, referred as Y_2O_3 , whose chemical composition is shown in Table 2. The existence of Y in the coating is to form Y_2O_3 to improve the adhesion between the Al_2O_3 scale and the coating [17,23]. No cracks or pores are detected on the coating/oxide scale interface, as shown in Figure 7b. This means that the oxidation resistance of the NiCrAlY coating is much better than the superalloy. However, the superalloy substrate beneath the NiCrAlY coating changed noticeably after oxidation for 100 h. An inter-diffusion zone (IDZ) and a secondary reaction zone (SRZ) were formed, as shown in Figure 7b. The thickness of the IDZ is about 2.3 μm , while the SRZ is beneath the IDZ, with a thickness of 52.1 μm . Due to the huge difference in the chemical composition between the coating and superalloy,

elemental interdiffusion between them occurs. Then, the IDZ and SRZ in the superalloy are formed. The chemical compositions in the coating and superalloy are listed in Table 2. Compared to the as-deposited coating and the superalloy, the Al and Cr contents in the interface are quite different. Al in the coating can diffuse out and react with oxygen in the environment, upon which a protective Al_2O_3 scale can be formed. Then, the content of Al in the coating decreased quickly, as shown in Figure 7d. At the same time, the Cr content in the coating is much higher than that in the superalloy substrate. This means that a large amount of Cr can diffuse from the coating into the substrate, which destroys the microstructural stability of the superalloy. Therefore, the IDZ, SRZ, and needle-like TCP phases are formed. The chemical compositions of the TCP phase are listed in Table 2. The content of refractory elements (Mo, W, and Re) is extremely high; they should originally be dissolved in the γ phase to improve the mechanical properties at high temperature. Then TCP phases are precipitated in the superalloy, which can be the source of crack initiation and the paths of crack propagation [17,24–28]. This indicates that the elemental interdiffusion between the NiCrAlY coating and the N5 superalloy during oxidation affects the life of the coating and the substrate superalloy. During oxidation, the diffusion of the antioxidant elements, such as Al and Cr, from the coating into the substrate decreases their contents in the coating. Therefore, they cannot maintain the stable growth of the oxide scale.

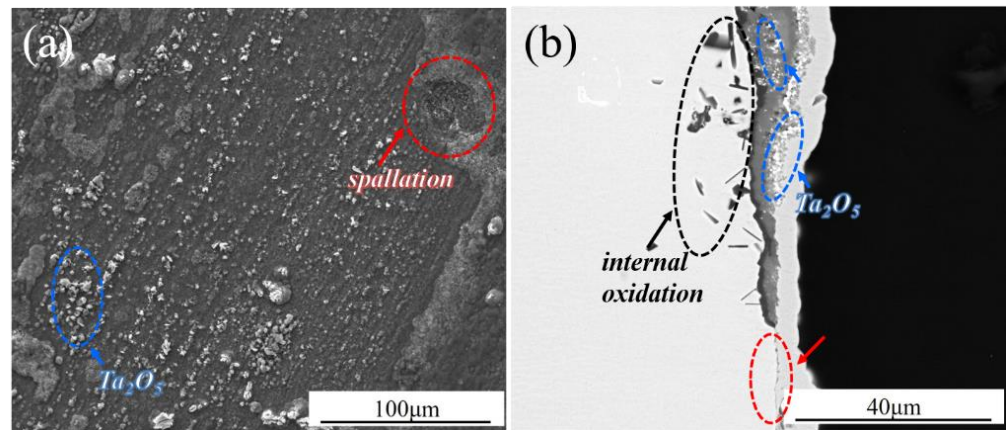


Figure 5. Microstructures of the superalloy after oxidation at 1050 °C for 100 h: (a) surface and (b) cross-section.

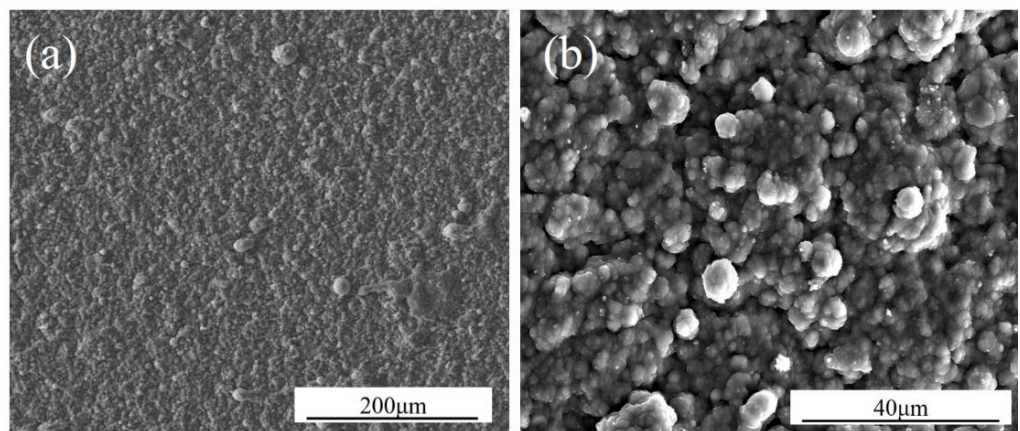


Figure 6. Surface microstructures of the NiCrAlY coating after oxidation at 1050 °C for 100 h: (a) at low magnification and (b) at high magnification.

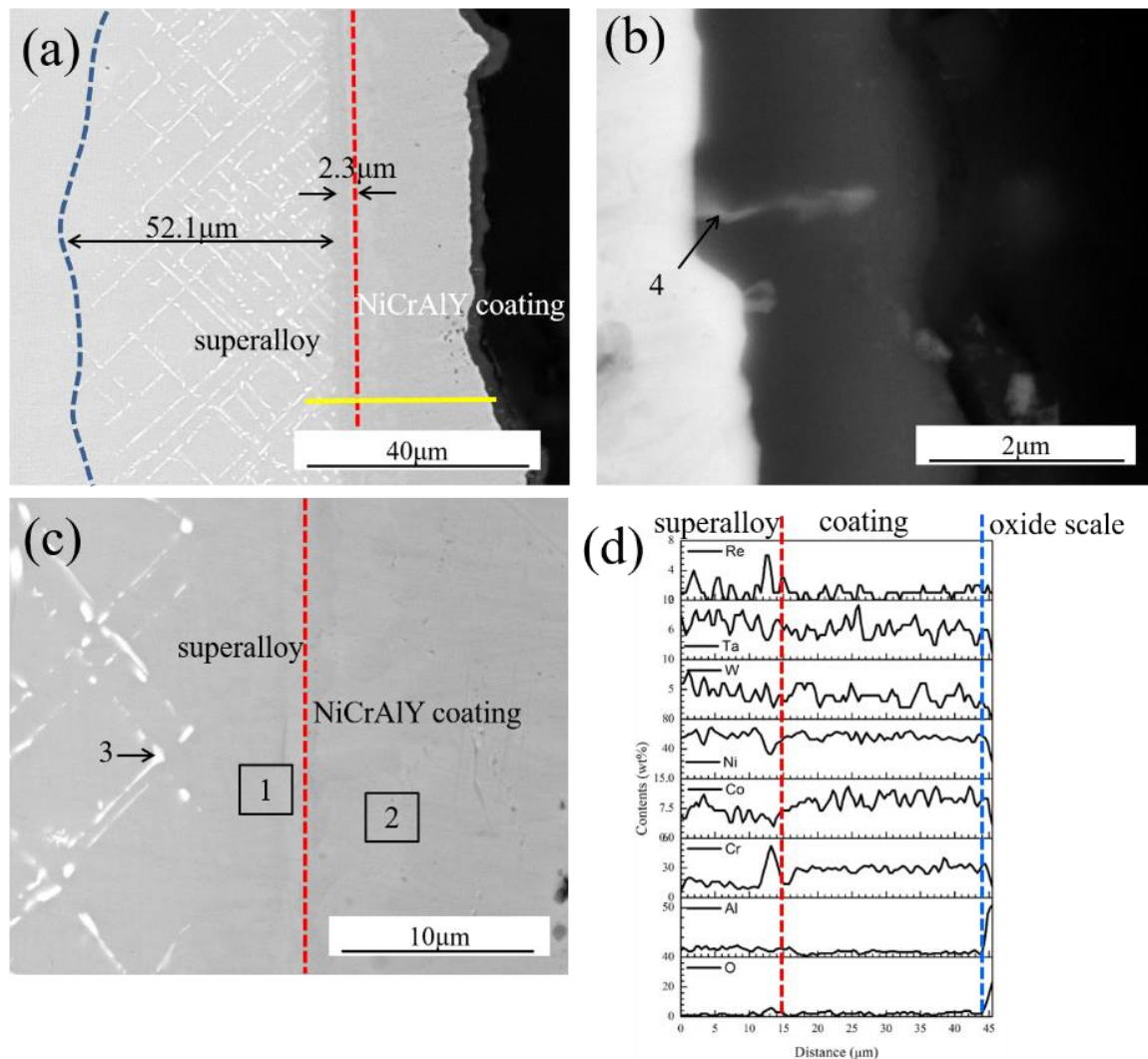


Figure 7. Cross-sectional microstructures and EDS line scanning of the NiCrAlY coating after oxidation at 1050 °C for 100 h: (a–c) cross-sectional microstructures and (d) EDS line scanning at yellow.

Table 2. Chemical compositions of “1”, “2”, and “3” in Figure 7 (wt.%).

	Ni	Co	Cr	Al	Ta	Mo	W	Re	O	Y
1	16.75	4.62	47.21	20.19	0.86	1.35	2.92	4.10	0	0
2	52.01	6.56	6.67	14.37	16.54	0.71	3.49	0	0	0
3	34.62	7.12	8.45	4.12	3.05	6.98	14.96	20.7	0	0
4	1.12	1.05	0.98	2.04	0	0	0	0	47.22	48.59

4. Conclusions

Al in the NiCrAlY coating fabricated by arc ion plating is included to form a protective Al_2O_3 scale and to improve the oxidation resistance of the superalloy at 1050 °C. At the same time, the chemical compositions of the coating and Ni-based single-crystal superalloy are clearly different, and elemental interdiffusion between them occurs. Al and Cr diffused from the coating to the superalloy substrate, while Ni, Mo, W, Re, etc. diffused from the superalloy substrate to the coating. As a result, the microstructure of the superalloy beneath the coating changes drastically. The IDZ and SRZ are detected. The IDZ is rich in Cr. A large number of needle-like TCP phases are found in the SRZ.

Author Contributions: Data curation, L.H.; Funding acquisition, L.Y. and Y.Q.; Investigation, Z.Z.; Methodology, L.Y.; Writing—original draft, L.H. and Z.Z.; Writing—review and editing, L.Y. and Y.Q. All authors have read and agreed to the published version of the manuscript.

Funding: This work was financially supported by the National Natural Science Foundation of China (Nos. 52001142) and Postgraduate Research & Practice Innovation Program of Jiangsu Province (No. KYCX22_3793).

Institutional Review Board Statement: Not applicable.

Informed Consent Statement: Not applicable.

Data Availability Statement: The data used to support the findings of this study are available from the corresponding author upon request.

Conflicts of Interest: The authors declare no conflict of interest.

References

1. Caron, P.; Khan, T. Improvement of Creep strength in a nickel-base single-crystal superalloy by heat treatment. *Mater. Sci. Eng.* **1983**, *61*, 173–184. [[CrossRef](#)]
2. Göbel, M.; Rahmel, A.; Schütze, M. The isothermal-oxidation behavior of several nickel-base single-crystal superalloys with and without coatings. *Oxid. Met.* **1993**, *39*, 231–261. [[CrossRef](#)]
3. Guo, D.; Zhao, L.; Jodoin, B. Cold spray for production of in-situ nanocrystalline MCrAlY coatings—Part II: Isothermal oxidation performance. *Surf. Coat. Technol.* **2021**, *409*, 126828. [[CrossRef](#)]
4. Bezencon, C.; Schnell, A.; Kurz, W. Epitaxial deposition of MCrAlY coatings on a Ni-base superalloy by laser cladding. *Scr. Mater.* **2003**, *49*, 705–709. [[CrossRef](#)]
5. Shi, L.; Xin, L.; Wang, X.; Wang, X.; Wei, H.; Zhu, S.L.; Wang, F.H. Influences of MCrAlY coatings on oxidation resistance of single crystal superalloy DD98M and their inter-diffusion behaviors. *J. Alloys Compd.* **2015**, *649*, 515–530. [[CrossRef](#)]
6. Drajewicz, M.; Kubaszek, T.; Kościelniak, B.; Góral, M.; Dziadosz, D. The isothermal oxidation of mcraly protective coatings. *Mater. Sci. Forum* **2021**, *1016*, 407–412. [[CrossRef](#)]
7. Demir, H.; Cosgun, A.E. The effect on energy efficiency of yttria-stabilized zirconia on brass, copper and hardened steel nozzle in additive manufacturing. *Coatings* **2022**, *12*, 690. [[CrossRef](#)]
8. Demir, H. The effects on thermal efficiency of yttria-stabilized zirconia and lanthanum zirconate-based thermal barrier coatings on aluminum heating black for 3D printer. *Coatings* **2021**, *11*, 792. [[CrossRef](#)]
9. Yuan, K.; Peng, R.L.; Li, X.H.; Johansson, S.; Wang, Y.D. Some aspects of elemental behaviour in HVOF MCrAlY coatings in high-temperature oxidation. *Surf. Coat. Technol.* **2015**, *261*, 86–101. [[CrossRef](#)]
10. Hua, C.; Song, P.; Huang, T.; He, X.; Li, C.; Zhai, R.; Li, Q.; Huang, W.; Lu, J. The growth mechanism of oxide scale with Pt on NiCoCrAlY coating in water vapor at 1050 °C. *Mod. Phys. Lett. B* **2021**, *35*, 2150111. [[CrossRef](#)]
11. Ghadami, F.; Aghdam, A.S.R.; Ghadami, S. Microstructural characteristics and oxidation behavior of the modified MCrAlX coatings: A critical review. *Vacuum* **2021**, *185*, 109980. [[CrossRef](#)]
12. Feuerstein, A.; Knapp, J.; Taylor, T.; Ashary, A.; Bolcavage, A.; Hitchman, N. Technical and economical aspects of current thermal barrier coating systems for gas turbine engines by thermal spray and EB-PVD: A Review. *J. Therm. Spray Technol.* **2008**, *17*, 199–213. [[CrossRef](#)]
13. Bobzin, K.; Wietheger, W.; Knoch, M.A. Development of thermal spray processes for depositing coatings on thermoplastics. *J. Therm. Spray Technol.* **2021**, *30*, 157–167. [[CrossRef](#)]
14. Kellai, A.; Kahla, S.; Dehimi, S.; Babes, B. Microstructural and mechanical properties of welding and thermal spraying coatings on ductile cast iron. *Defect Diffus. Forum* **2021**, *406*, 300–311. [[CrossRef](#)]
15. Yang, L.L.; Gao, F.Y.; Zhou, Z.H.; Jia, Y.X.; Du, Y.; Wang, J.L.; Qiao, Y.X.; Zhu, S.L.; Wang, F.H. Oxidation behavior of the AlN coatings on the TiAl alloy at 900 °C. *Corros. Sci.* **2022**, *in press*. [[CrossRef](#)]
16. Guo, M.H.; Wang, Q.M.; Ke, P.L.; Gong, J.; Sun, C.; Huang, R.F.; Wen, L.S. The preparation and hot corrosion resistance of gradient NiCoCrAlYSiB coatings. *Surf. Coat. Technol.* **2006**, *200*, 3942–3949. [[CrossRef](#)]
17. Yang, L.L.; Chen, M.H.; Wang, J.L.; Qiao, Y.X.; Guo, P.Y.; Zhu, S.L.; Wang, F.H. Microstructure and composition evolution of a single-crystal superalloy caused by elements interdiffusion with an overlay NiCrAlY coating on oxidation. *J. Mater. Sci. Technol.* **2020**, *45*, 49–58. [[CrossRef](#)]
18. Xie, S.; Lin, S.; Shi, Q.; Wang, W.; Song, C.; Xu, W.; Dai, M. A study on the mechanical and thermal shock properties of MCrAlY coating prepared by arc ion plating. *Surf. Coat. Technol.* **2021**, *413*, 127092. [[CrossRef](#)]
19. Meng, B.; Wang, J.L.; Yang, L.L.; Chen, M.H.; Zhu, S.L.; Wang, F.H. On the rumpling mechanism in nanocrystalline coatings: Improved by reactive magnetron sputtering with oxygen. *J. Mater. Sci. Technol.* **2023**, *132*, 69–80. [[CrossRef](#)]
20. Meng, B.; Wang, J.L.; Yang, L.L.; Zhu, L.J.; Chen, M.H.; Zhu, S.L.; Wang, F.H. Influence of fuel combustion on the corrosion behavior of pipeline steels in fire flooding technology. *NPJ Mater. Degrad.* **2022**, *21*, 6. [[CrossRef](#)]

21. Ren, P.; Yang, Y.F.; Li, W.; Zhu, S.L.; Wang, F.H. Cyclic oxidation behavior of a multilayer composite coating for single crystal superalloys. *Corros. Sci.* **2018**, *145*, 26–34. [[CrossRef](#)]
22. Wang, J.L.; Chen, M.H.; Zhu, S.L.; Wang, F.H. Ta effect on oxidation of a nickel-based single-crystal superalloy and its sputtered nanocrystalline coating at 900–1100 °C. *Appl. Surf. Sci.* **2015**, *345*, 194–203. [[CrossRef](#)]
23. Wang, J.L.; Chen, M.H.; Yang, L.L.; Zhu, S.L.; Wang, F.H. Comparative study of oxidation and interdiffusion behavior of AlP NiCrAlY and sputtered nanocrystalline coatings on a nickel-based single-crystal superalloy. *Corros. Sci.* **2015**, *98*, 530–540. [[CrossRef](#)]
24. Yang, L.L.; Zhou, Z.H.; Yang, R.Z.; Wang, J.L.; Chen, M.H.; Qiao, Y.X.; Zhu, S.L.; Wang, F.H. Effect of Al and Cr on the oxidation behavior of nanocrystalline coatings at 1050 °C. *Corros. Sci.* **2022**, *200*, 110191. [[CrossRef](#)]
25. Xiao, Q.; Huang, Q.Y.; Yang, L.L.; Ren, P.; Wang, Q.W.; Yang, Y.F.; Li, W.; Zhu, S.L.; Wang, F.H. The cyclic oxidation behavior of a Pt modified γ' nanocrystalline coating at 1150 °C. *Corros. Sci.* **2022**, *208*, 110638. [[CrossRef](#)]
26. Yang, S.S.; Li, S.; Wang, J.L.; Bao, Z.; Yang, L.L.; Chen, M.H.; Zhu, S.L.; Wang, F.H. A novel single-phase γ' nanocrystalline coating with high resistance to oxidation and scale rumpling yet mitigated interdiffusion with the alloy substrate. *Corros. Sci.* **2021**, *192*, 109866. [[CrossRef](#)]
27. Yang, L.L.; Wang, J.L.; Yang, R.; Yang, S.; Jia, Y.; Chen, M.; Qiao, Y.X.; Guo, P.; Zhu, S.L.; Wang, F.H. Oxidation behavior of a nanocrystalline coating with low Ta content at high temperature. *Corros. Sci.* **2021**, *180*, 109182. [[CrossRef](#)]
28. Huang, D.; Qiao, Y.X.; Yang, L.L.; Wang, J.L.; Chen, M.H.; Zhu, S.L.; Wang, F.H. Effect of shot peening of substrate surface on cyclic oxidation behavior of sputtered nanocrystalline coating. *Acta Metall. Sin.* **2022**, in press. [[CrossRef](#)]

Disclaimer/Publisher's Note: The statements, opinions and data contained in all publications are solely those of the individual author(s) and contributor(s) and not of MDPI and/or the editor(s). MDPI and/or the editor(s) disclaim responsibility for any injury to people or property resulting from any ideas, methods, instructions or products referred to in the content.